RESEARCH ARTICLE

Myotomy technique and esophageal contractility impact blown-out myotomy formation in achalasia: an in silico investigation

© Sourav Halder,¹ © Shashank Acharya,² Wenjun Kou,³ Ryan A. J Campagna,⁴ Joseph R. Triggs,⁵ Dustin A. Carlson,³ Abdul Aziz Aadam,³ Eric S. Hungness,⁴ Peter J. Kahrilas,³ John E. Pandolfino,³ and © Neelesh A. Patankar^{1,2}

Abstract

We used in silico models to investigate the impact of the dimensions of myotomy, contraction pattern, the tone of the esophago-gastric junction (EGJ), and musculature at the myotomy site on esophageal wall stresses potentially leading to the formation of a blown-out myotomy (BOM). We performed three sets of simulations with an in silico esophagus model, wherein the myotomy-influenced region was modeled as an elliptical section devoid of muscle fibers. These sets investigated the effects of the dimensions of myotomy, differing esophageal contraction types, and differing esophagogastric junction (EGJ) tone and wall stiffness at the myotomy affected region on esophageal wall stresses potentially leading to BOM. Longer myotomy was found to be accompanied by a higher bolus volume accumulated at the myotomy site. With respect to esophageal contractions, deformation at the myotomy site was greatest with propagated peristalsis, followed by combined peristalsis and spasm, and pan-esophageal pressurization. Stronger EGJ tone with respect to the wall stiffness at the myotomy site was found to aid in increasing deformation at the myotomy site. In addition, we found that an esophagus with a shorter myotomy performed better at emptying the bolus than that with a longer myotomy. Shorter myotomies decrease the chance of BOM formation. Propagated peristalsis with EGJ outflow obstruction has the highest chance of BOM formation. We also found that abnormal residual EGJ tone may be a co-factor in the development of BOM, whereas remnant muscle fibers at myotomy site reduce the risk of BOM formation.

NEW & NOTEWORTHY Blown-out myotomy (BOM) is a complication observed after myotomy, which is performed to treat achalasia. In silico simulations were performed to identify the factors leading to BOM formation. We found that a short myotomy that is not transmural and has some structural architecture intact reduces the risk of BOM formation. In addition, we found that high esophagogastric junction tone due to fundoplication is found to increase the risk of BOM formation.

achalasia; diverticulum; Heller myotomy; dysphagia

INTRODUCTION

Achalasia is an esophageal motility disorder characterized by impaired esophagogastric junction (EGJ) relaxation and absent peristalsis. The Chicago classification (1, 2) categorizes achalasia into subtypes I, II, and III based on pressure topography patterns observed with high-resolution manometry (HRM). A recent study (3) showed that the incidence and prevalence of achalasia diagnosed using high-resolution manometry is at least two- to threefold greater than previous estimates with an incidence in the range of 2–3/100,000 and a steadily rising prevalence as newly diagnosed cases accumulate. The standard surgical treatment of achalasia is laparoscopic Heller myotomy (LHM) during which the circular

muscle (CM) fibers of the distal esophagus and lower esophageal sphincter (LES) are disrupted. Figure 1A shows three sequential time points during a LHM procedure. The myotomy extends for a variable length onto the distal esophagus and gastric cardia (4). Because myotomy can lead to uncontrolled reflux, it is usually combined with a partial fundoplication (5), wherein the gastric fundus is mobilized and partially wrapped around the LES to reduce the severity of postprocedure reflux.

Another potential complication of myotomy is the formation of a blown-out myotomy (BOM) in the distal esophagus (6, 7). A BOM is a pseudodiverticulum in the distal esophagus that can progressively enlarge and compromise esophageal emptying, potentially mandating further surgery (Fig.



¹Theoretical and Applied Mechanics Program, McCormick School of Engineering, Northwestern University, Evanston, Illinois; ²Department of Mechanical Engineering, McCormick School of Engineering, Northwestern University, Evanston, Illinois; ³Division of Gastroenterology and Hepatology, Department of Medicine, Feinberg School of Medicine, Northwestern University, Chicago, Illinois; ⁴Department of Surgery, Feinberg School of Medicine, Northwestern University, Chicago, Illinois; and ⁵Division of Gastroenterology, Perelman School of Medicine, University of Pennsylvania, Philadelphia, Pennsylvania

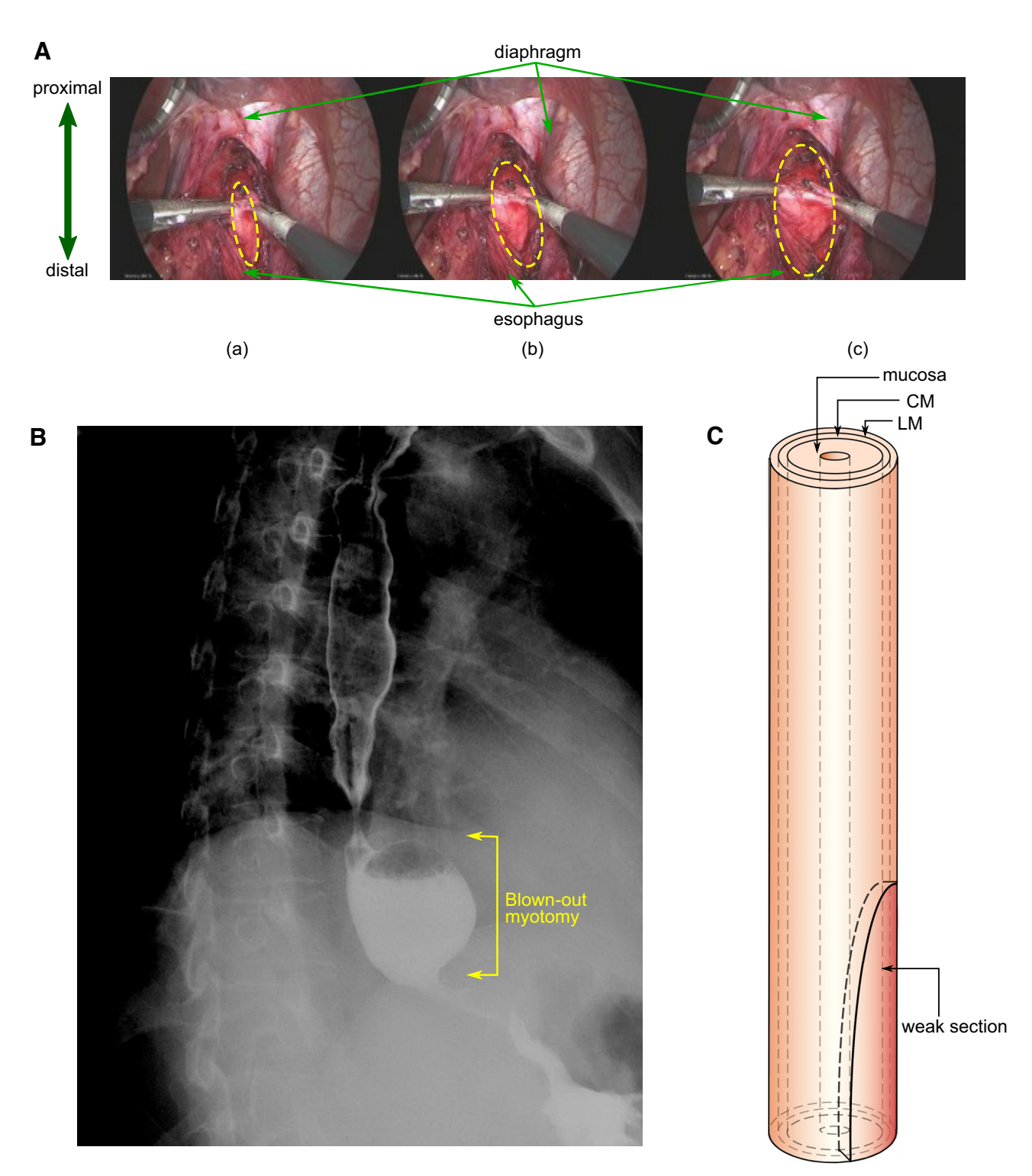


Figure 1. *A*: laparoscopic Heller myotomy. Distal esophagus during laparoscopic myotomy is shown. *Top*: the diaphragmatic crus arcing over the esophagus. The longitudinal muscle is separated, and the circular muscle is broken. The myotomy region takes the form of an ellipse. The upper half of the ellipse approximately extends from the LES to the distal esophagus. The lower half of the weak section extends from the LES into the stomach. a–c) three times during the myotomy are presented. The dashed yellow ellipses show the enlarging area of bared mucosa with progression of the myotomy. Maximum extension of the opened grasper (=2 cm) was used as a scale to calculate to the dimensions of myotomy and diameter of the esophagus. B: esophagram of a blown out myotomy (BOM). BOM formed in the patient after myotomy just above the diaphragm with the EGJ observed as the narrow region distal to the BOM. Barium is retained inside the pseudodiverticulum, almost filling it. C: vEsophagus model used in our simulations with three layers: LM, CM, and mucosa. The weakened region from the myotomy is shown as an ellipse at the distal end. During myotomy, the LM fibers are loosened and their connectivity with each other is disrupted; the CM fibers are broken. The matrix in which the muscle fibers are embedded remains in place, although its connection with the fibers might be broken. To model this behavior, we removed the muscle fibers in the CM and LM in an elliptical region near the distal end of the esophagus. We have modeled the myotomy affected region by weakening a half-elliptical section at the distal end of the esophagus (since the lower half extends into the stomach). CM, circular muscle; EGJ, esophagogastric junction; LES, lower esophageal sphincter; LM, longitudinal muscle.

1B). BOM is characterized by an outward protrusion of the mucosa through the defect in the muscle layers resultant from the myotomy. BOM formation can be attributed to a complex combination of physical and biological factors such as strength of the esophageal wall after myotomy, elastic and plastic behavior of the esophagus wall, remodeling, and neural-activated peristaltic contraction strength. In this work, we investigated the underlying physics potentially leading to the formation of BOM using a fully coupled three-dimensional in silico model called virtual esophagus (vEsophagus). A previous study using a computational model of the esophagus analyzed the effect of anatomical asymmetry, tissue anisotropy, and the LES in the formation of epiphrenic diverticula (8). We used a similar model to understand the impact of the dimensions of myotomy in the formation of BOMs. Furthermore, although myotomy obliterates the LES, there is some residual tone at the esophagogastric junction (EGJ) attributable to the crural diaphragm, the remains of the esophageal wall at the myotomy site, and the associated partial fundoplication. The impact of this collective tone at the EGJ in the formation of BOM was also investigated and described in the following sections.

MATERIALS AND METHODS

vEsophagus: In Silico Model of the Esophagus

The vEsophagus was modeled as a multilayered axisymmetric cylindrical tube as shown in Fig. 1C. It is a computational model that captures the fluid-structure interaction between the esophageal walls and the swallowed bolus using the immersed boundary (IB). This model was based on a previous work (9), and the mathematical details of the vEsophagus are provided in the APPENDIX. Because of the use of the IB method, the vEsophagus wall has a viscoelastic nature, which is also observed in reality (10, 11).

The dimensions of the vEsophagus were based on a typical LHM video, a few instants of which are shown in Fig. 1A. The maximum extension of the opened grasper is 2 cm. Using that as a scale, we estimated the average outer diameter of the collapsed esophagus to be 1.6 cm. The vEsophagus wall was composed of three main layers: mucosa (which includes both mucosa and submucosa), circular muscle (CM), and longitudinal muscles (LMs). The approximate thickness of each layer was estimated experimentally in a previous study (12). Using the same relative ratios of the layers, we calculated the CM and LM thickness to be ~1 mm each and mucosal thickness to be 5.5 mm. For our simulations, we assumed the total length of the esophagus including the upper esophageal sphincter (UES) and LES to be 24 cm. The UES and LES were assumed 3 cm each. The UES opens for a brief interval during a swallow to allow bolus entry into the esophagus and then closes for the duration of the sequence (13, 14). Hence, in our simulations, we eliminated the UES by assuming the proximal end of the vEsophagus to be fixed and only considered the esophagus distal to the UES.

The wall of the vEsophagus was modeled as a composite of hyperelastic materials with each layer composed of fibers embedded in a matrix (15, 16). The hyperelastic behavior of the vEsophagus wall layers was defined in other in silico models (9, 17–19) and discussed in APPENDIX.

Simulation Details

We performed three sets of simulations to investigate the effect of myotomy on the pressure stresses that can potentially lead to the formation of a BOM. First, we did a parametric study with five cases with different myotomy dimensions, specifically the length and width of the weakened section. Table 1 shows the details of different cases simulated. In all cases, we assumed the extreme case, wherein the LES remained occluded. This helped to quantify the effect of myotomy as a set of baseline cases that were not influenced by other physiological factors. Since we assumed the EGJ to be fully occluded in these first simulations, we eliminated the LES in the vEsophagus, leaving 18 cm of esophagus between the UES and LES, fixed at both ends. The lengths of the myotomies specified in Table 1 are considered from the proximal end of the LES. Thus, the total lengths of the myotomies were 3 cm more than shown in Table 1. The contraction pattern was kept the same for all five cases (pan-esophageal pressurization) for comparison.

Second, we investigated the effect of four different physiologically motivated esophageal muscle contraction patterns that can potentially lead to the formation of a BOM: normal peristalsis, minimal/no contraction as observed in achalasia type I, pan-esophageal contraction as observed in achalasia type II, and peristalsis transitioned into distal spasm i.e., spasm in the distal half of the esophagus, which predominantly contains smooth muscles, as observed in achalasia type III. These contraction patterns are neurally controlled manifest by the circumferential contraction of the CM and the longitudinal shortening of the LM (20, 21). The details of these cases are given in Table 2. All these cases model EGJ outflow obstruction (EGJOO) by a closed distal end. We performed two sets of this simulation, one with the standard reference length of 6 cm, and the other with a short myotomy length of 2 cm to describe the difference in outcome of myotomv length.

Third, we investigated the effect of EGJ tone and remnant musculature at the myotomy site on pressure stresses that can potentially lead to the formation of a BOM by considering two groups with six cases for group I and one case of group II as detailed in Table 3. Since the LES is obliterated by the myotomy, the EGJ tone can be contributed to external anatomical features such as the hiatus and a fundoplication. This EGJ tone was modeled as increased stiffness at a short section of the distal esophagus. This is reasonable as the effective impact of the EGJ tone in HRM and EndoFLIP appears as a region of higher stiffness by providing more resistance to opening compared with the remainder of the esophagus. Although the muscle fibers are damaged at the myotomy site, the wall stiffness at that site might not

Table 1. Dimensions of elliptical myotomy section in simulation set 1

Case Number	1/2 Major Axis, mm	Minor Axis, mm
1	60	7
2	90	7
3	30	7
4	60	4
5	60	10

Table 2. Details for simulation set 2

Case Number	Contraction Type	Details	
1	Peristalsis (normal), standard myotomy	Contraction width: 6 cm, speed: 2 cm/s, EGJOO, myotomy length: 6 cm	
2	Very weak contraction (achalasia I), standard myotomy	Stationary over the entire esophageal length, EGJOO, myotomy length: 6 cm	
3	Pan-esophageal contraction (achalasia II), stand- ard myotomy	Stationary over the entire esophageal length with weak irregularities in strength along the length, EGJOO, myotomy length: 6 cm	
4	Proximal peristalsis transitions with distal spasm (achalasia III), standard myotomy	Peristalsis in the proximal half of the esophagus that merges with spasm (three stationary peaks) in the distal half, EGJOO, myotomy length: 6 cm	
5	Peristalsis (normal), short myotomy	Contraction width: 6 cm, speed: 2 cm/s, EGJOO, myotomy length: 2 cm	
6	Very weak contraction (achalasia I), short myotomy	Stationary over the entire esophageal length, EGJOO, myotomy length: 2 cm	
7	Pan-esophageal contraction (achalasia II), short myotomy	Stationary over the entire esophageal length with weak irregularities in strength along the length, EGJOO, myotomy length: 2 cm	
8	Proximal peristalsis transitions with distal spasm (achalasia III), short myotomy	Peristalsis in the proximal half of the esophagus that merges with spasm (3 stationary peaks) in the distal half, EGJOO, myotomy length: 2 cm	

EGJOO, esophagogastric junction outflow obstruction.

necessarily be equal to the strength of the mucosa. This is because some remnant muscle fibers might be present after myotomy. In addition, the myotomy site might heal or scar to some extent with time, which can raise the stiffness of the wall at the myotomy site. The total length of the esophagus in these cases was 21 cm since the LES was included and the lower end of the esophagus was free to move.

In reality, the factors discussed in this section (myotomy dimensions, contraction pattern, and EGJ tone) work together making it impossible to investigate their individual impact. The simulation sets described in this section addresses this problem by systematically investigating the impact of varying each factor independently while holding the others constant.

Details of Numerical Simulation

The numerical simulations were performed using the immersed boundary method adaptive mesh refinement (IBAMR) software infrastructure (22). For postprocessing and visualization of the simulation results, we used an opensource visualization software VisIt (23).

RESULTS

Simulation Set 1: Parametric Study of the Effect of Myotomy with Fully Occluded EGJ

The deformation of the esophagus during bolus transport for the cases detailed in Table 1 is shown in Fig. 2 for the same time instant. Case 1 used the dimensions of the weakened section estimated from the LHM video as shown by Fig. 1A and is used as a reference for comparison with the other cases. Physiologically, the conditions for this simulation set are similar to an incomplete myotomy or tight fundoplication performed on a patient with type II achalasia.

Cases 1, 2, and 3 had a maximum outward displacement at the myotomy site of 9.5 mm, 9.2 mm, and 9.3 mm, respectively. Thus, although both increasing and decreasing the length of myotomy from the reference case 1, reduced the degree of deformation, the difference in the magnitude of maximum outward displacement was minimal. The percentage volume of fluid accumulated in the myotomy affects the region with respect to the total bolus volume for cases 1, 2, and 3 were found to be 48.6%, 67.6%, and 28.7%, respectively. Thus, the volume of fluid that accumulated inside the myotomy was proportional to the length of myotomy.

Cases 1, 4, and 5 had varying minor axes, and the maximum displacements were 9.5 mm, 9.6 mm, and 9.7 mm, respectively. As with the cases with varied myotomy lengths, the differences were minimal. The percentage volume of fluid accumulated in the myotomy affect the region with respect to the total bolus volume for cases 1, 4, and 5 were found to be 48.6%, 48.8%, and 48.4%, respectively. Thus, the volume of fluid that accumulated inside the myotomy site was also very similar as can be seen in Fig. 2.

Table 3. Details for simulation set 3

Case Number	Group I				
1	Standard myotomy length (6 cm); no EGJ tone; myotomy affected zone walled by mucosa only; contraction type: normal peristalsis				
2	Standard myotomy length (6 cm); with an EGJ tone; myotomy affected zone walled by mucosa only; contraction type: normal peristalsis				
3	Standard myotomy length (6 cm); with an EGJ tone; myotomy affected zone walled by mucosa and weakened muscle layers (the strength of the muscle fibers were reduced by 99%, but the matrix of the muscle layers were intact at the myotomy site); contract tion type: normal peristalsis				
4	Short myotomy length (3 cm); no EGJ tone; myotomy affected zone walled by mucosa only; contraction type: normal peristalsis				
5	Short myotomy length (3 cm); with an EGJ tone; myotomy affected zone walled by mucosa only; contraction type: normal peristals				
6	6 Short myotomy length (3 cm); with an EGJ tone; myotomy affected zone walled by mucosa and weakened muscle layers (the strength of the muscle fibers were reduced by 99% but the matrix of the muscle layers were intact at the myotomy site); contribution type: normal peristalsis				
	Group II				
POEM length: 12 cm; LM intact at the myotomy site while CM fibers were broken, and CM matrix strength reduced 100-fold; with an EGJ tone; co traction type: normal peristalsis					

CM, circular muscle; EGJ, esophagogastric junction; LM, longitudinal muscle; POEM, Peroral endoscopic myotomy.

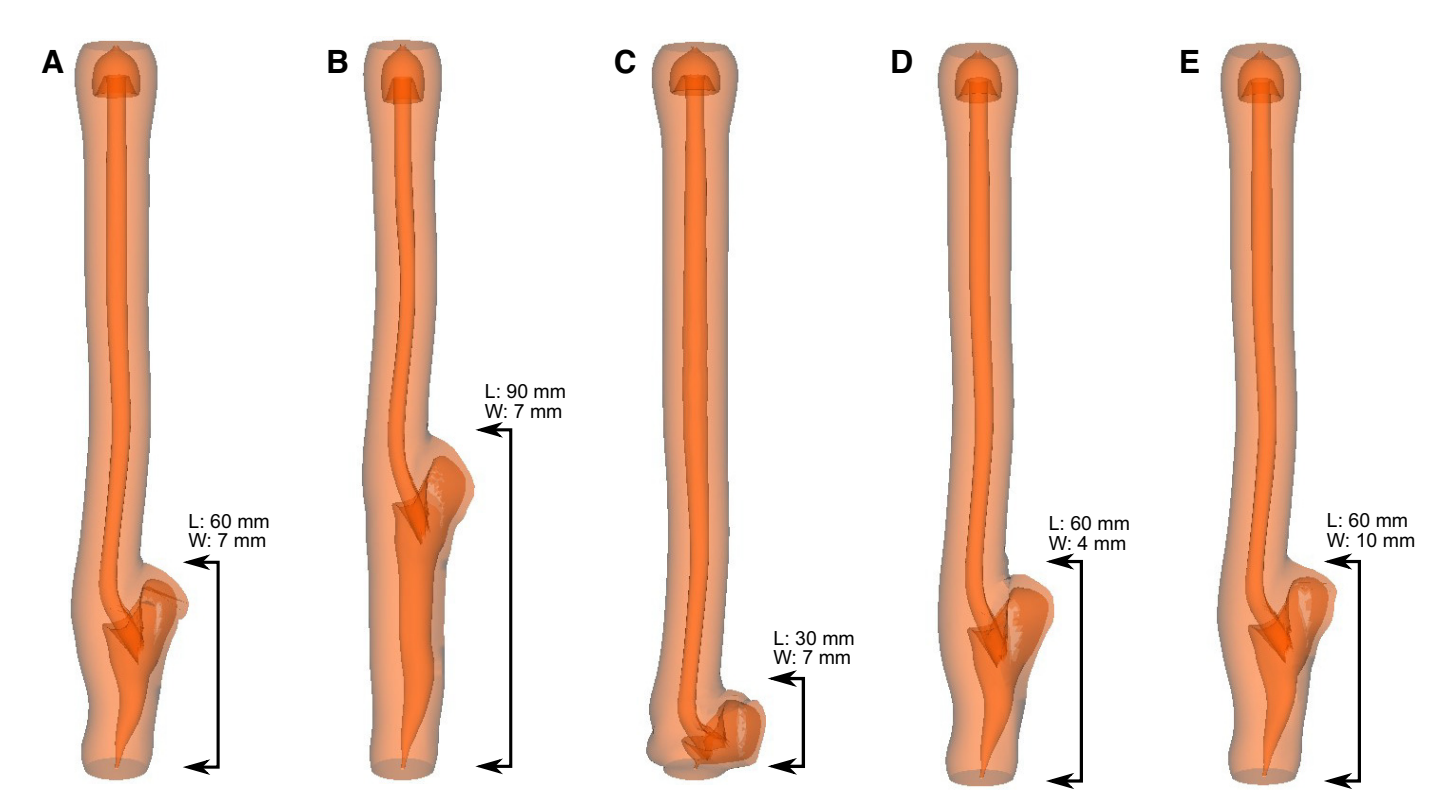


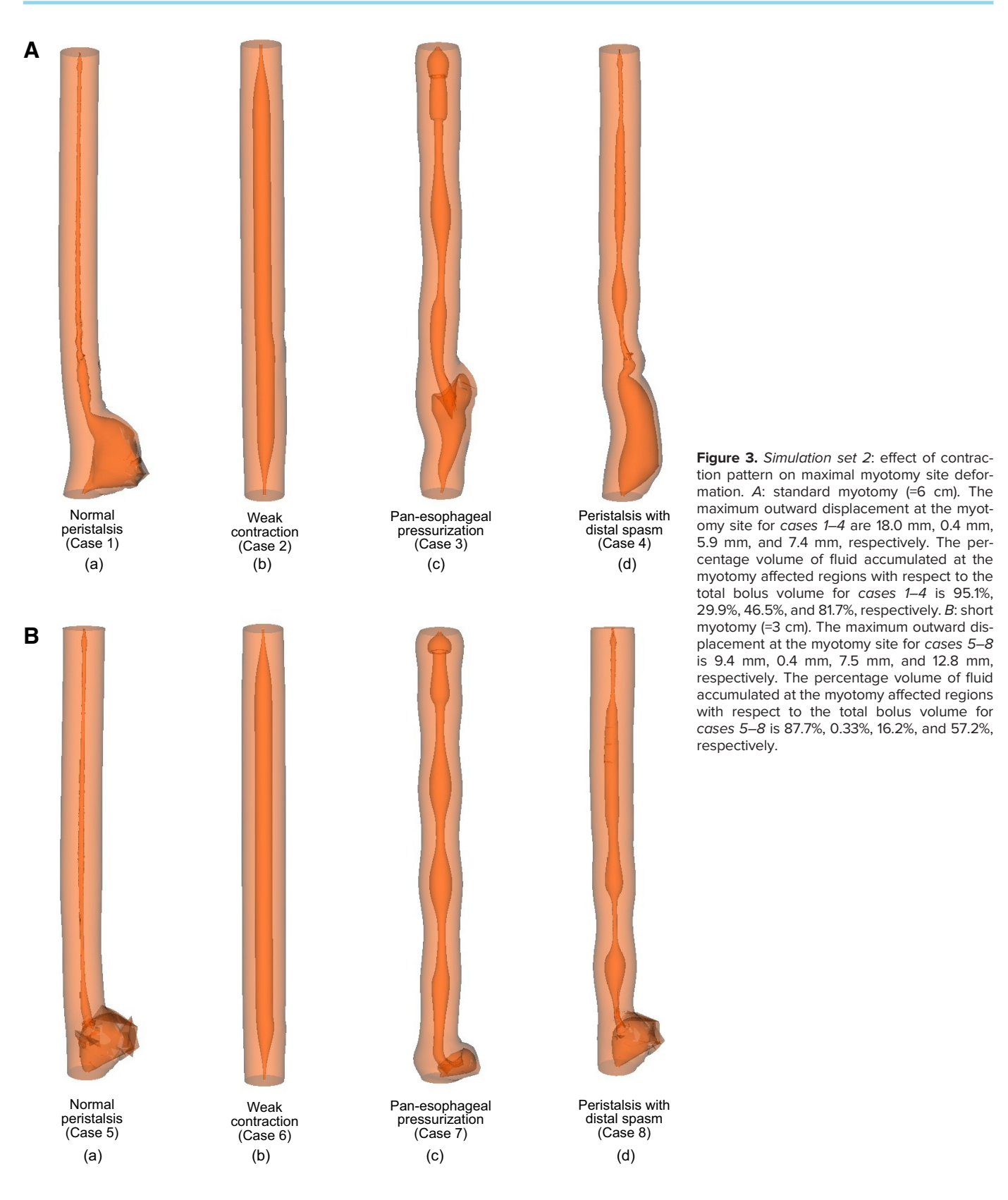
Figure 2. Simulation set 1: myotomy site deformation with different dimensions of myotomy. A: length 60 mm, max width 7 mm. B: length 90 mm, max width 7 mm. C: length 30 mm, max width 7 mm. D: length 60 mm, max width 4 mm. E: length 60 mm, max width 10 mm. A-E shows the deformed shape of the esophagus for cases 1–5, respectively at the same time instant. The maximum outward displacement at the myotomy site for cases 1–5 is 9.5 mm, 9.2 mm, 9.3 mm, 9.6 mm, and 9.7 mm, respectively. The percentage volume of fluid accumulated at the myotomy affected regions with respect to the total bolus volume for cases 1–4 is 48.6%, 67.6%, 28.7%, 48.8%, and 48.4%, respectively.

Simulation Set 2: Effect of Muscle Contraction

The maximal deformation at the myotomy site associated with the four different patterns of esophageal contraction detailed in Table 2 is shown in Fig. 3. The maximum outward displacement at the standard myotomy site for *cases* 1–4 was found to be 18.0 mm, 0.4 mm, 5.9 mm, and 7.4 mm, respectively. The percentage volume of fluid accumulated at the myotomy affected regions with respect to the total bolus volume for these cases was 95.1%, 29.9%, 46.5%, and 81.7%, respectively. The maximum outward displacement at the short myotomy site for cases 5-8 is 9.4 mm, 0.4 mm, 7.5 mm, and 12.8 mm, respectively. The percentage volume of fluid accumulated at the short myotomy affected regions with respect to the total bolus volume for cases 5-8 is 87.7%, 0.33%, 16.2%, and 57.2%, respectively. Thus, the volume of fluid accumulated at the myotomy site for short myotomy was less compared with that for a longer myotomy. On comparing these cases, we observed that the maximum outward displacement at the myotomy occurred with normal peristalsis. In addition, the peristaltic contraction passed over the weakened section without collapsing the outward protrusion, but rather, increased its outward displacement, and aided the deformation at the myotomy site as shown in Fig. 3Aa and Ba. No prominent deformation at the myotomy site was observed for cases 2 and 6. The pan-esophageal pressurization of cases 3 and 7 does not lead to efficient transport of the bolus from the proximal to the distal esophagus as evident by the remnant fluid at the proximal esophagus. The BOMs formed in these cases had lesser volumes compared with *cases 1, 4, 5*, and *case 8. Cases 4* and 8 show that proximal normal peristalsis, which transitioned into distal spasms, resulted in volumes accumulated at the myotomy site less than *cases 1* and 4, but greater than the other cases. The effect of distal spasm in shorter myotomy was more prominent compared with that observed for longer myotomy as observed by comparing the shape of the bolus in Fig. 3Ad and Bd. Because of the lack of contractions, there was no prominent deformation at the myotomy site for *case 6* just like *case 2*.

Simulation Set 3 (Group I): Effect of EGJ Tone and Musculature at the Myotomy Site

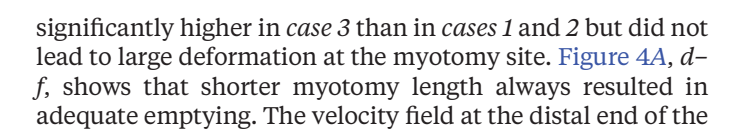
The effect of varied EGJ tone and remnant muscle fibers at the myotomy site on deformation at the myotomy affected zone was investigated by comparing six cases as detailed in Table 3. Figure 4 shows bolus transport through an esophagus with a standard size myotomy (Fig. 4, A–C, a–c) and with a short myotomy (Fig. 4, A–C, d–f). When comparing $cases\ 1$ and a2, we see that without EGJ tone the peristaltic contraction successfully emptied the esophagus in $case\ 1$, but because of the presence of the EGJ tone in $case\ 2$, a prominent deformation at the myotomy site was observed. But, as we see in Fig. a0, even with the presence of the EGJ tone, the esophagus with a stronger wall at the myotomy site was able to empty with the help of a peristaltic contraction without a prominent deformation at the myotomy location. In



addition, Fig. 4B, a–c, illustrates the bolus emptying in *cases* 1 and 3 by the high fluid velocity at the distal end of the esophagus, and the negligible emptying of *case* 2 by almost no fluid flow at the distal end and the accumulated fluid at

the myotomy location. Figure 4C, a and b, shows that the intrabolus pressure reached a higher value for $case\ 2$ compared with $case\ 1$ and led to a prominent deformation at the myotomy site in $case\ 2$. The intrabolus pressure was

Figure 4. Simulation set 3 (group I): effect of EGJ tone and myotomy site muscle architecture on myotomy site deformation. A: a-f) myotomy deformation associated with cases 1-6, respectively. The esophagus empties in all the cases except case 2 with very little deformation at the myotomy site. The esophagus in case 2 has negligible emptying and the bolus accumulates in the myotomy site proximal to the EGJ. The volume of the bolus inside the esophagus at the end of the simulation for cases 1-6 is 37.9%, 98.1%, 15.0%, 15.9%, 13.3%, and 11.5% of the initial bolus volume, respectively. B: nondimensional velocity distribution within the esophagus with a myotomy at the same time instant. a-f illustrate cases 1-6, respectively. All the cases except case 2 show bolus emptying evident from the high fluid flow rate at the distal end of the esophagus. In case 2, only a negligible amount of bolus fluid leaves the esophagus and most of it stays accumulated at the myotomy site. C: nondimensional pressure distribution within the esophagus with a myotomy at the same time instant. a-f illustrate cases 1-6, respectively. The intrabolus pressure (IBP) is higher in case 2 than in case 1. The average IBP in case 2 is 33% higher than case 1. Cases 3-6 have significantly higher IBP. The IBP of cases 3-6 is 7.3, 7.4, 8.1, and 8.9 times that of case 1, respectively. EGJ, esophagogastric junction.



esophagus as shown in Fig. 4*B*, *d*–*f*, demonstrates the emptying process. In addition, Fig. 4*C*, *d*–*f*, shows that the intrabolus pressure in *cases* 4–6 was higher compared with that observed in *cases* 1 and 2. As shown in Fig. 4*A*, the volumes

of the bolus accumulated inside the esophagus at the end of the simulation for cases 1-6 were 37.9%, 98.1%, 15.0%, 15.9%, 13.3%, and 11.5% of the initial bolus volume, respectively. For the time instant shown in Fig. 4C, the average intrabolus pressure in case 2 was 33% higher than case 1. Cases 3-6 had significantly higher intrabolus pressure than cases 1 and 2. We found that the average intrabolus pressure of cases 3-6 were 7.3, 7.4, 8.1, and 8.9 times that of *case 1*, respectively.

Simulation Set 3 (Group II): Effect of POEM at the **Myotomy Site**

Cases 3 and 6 of group I demonstrated that the esophagus with greater stiffness at the myotomy site compared with the other cases resisted deformation at the myotomy site and aided in bolus emptying. In LHM both CM and LM fibers are obliterated resulting in a very weak esophageal wall at the myotomy site. Peroral endoscopic myotomy (POEM), on the other hand, only obliterates the CM fibers and leaves the LM

intact increasing the wall strength at the myotomy site compared with that seen with LHM. Group II simulation investigates the impact of POEM on BOM formation and bolus emptying. Figure 5A shows the final configuration of the vEsophagus after bolus transport. The high-velocity field at one instant, as shown by Fig. 5B, describes how the bolus empties out of the esophagus by the peristaltic contraction. The high intrabolus pressure (shown by Fig. 5C) drives the fluid out of the esophagus. The intrabolus pressure, in this case, was 5.3 times higher than that of case 1 of group I (which was used as a reference for the other simulations in simulation set 3).

DISCUSSION

We performed three sets of simulations with an in silico model called vEsophagus to analyze the effect of myotomy dimensions, esophageal contraction pattern, and EGJ outflow

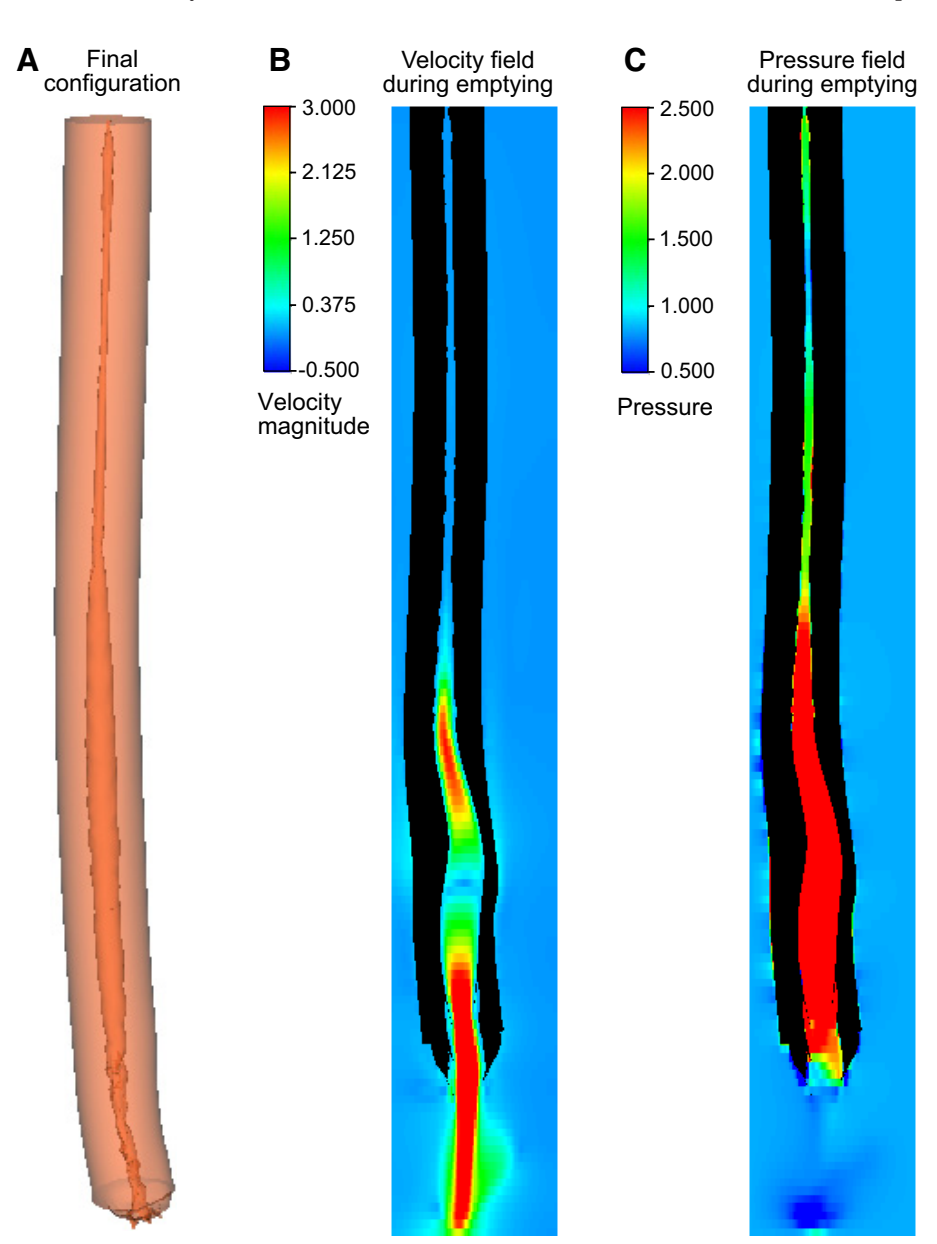


Figure 5. Simulation set 3 (group II): effect of POEM on the myotomy site deformation. A: the final configuration of the esophagus undergone with POEM. No prominent deformation observed at the myotomy site. B and C: the velocity and pressure fields inside the esophagus at a time instant when the EGJ opens due to the intrabolus pressure, and the bolus empties out of the esophagus. The IBP in this case is 5.3 times that of case 1 of group I (which was used as a reference). IBP, intrabolus pressure; POEM, Peroral endoscopic myotomy.

resistance on the pressure stresses leading to BOM formation. In all these simulations, the myotomy affected region was modeled by weakening the muscle layers in a half-elliptical weak section at the distal end of the vEsophagus. From simulation set 1, we found that increasing the length of the myotomy increases the chances of formation of a BOM, whereas varying the width of the myotomy did not have a significant impact on the size of the BOM. Since the esophagus anatomy is long and narrow, there is more scope for the variation in the length of myotomy in comparison to the width. Thus, the impact of variation of length on the likely formation of a BOM is more important compared with the variation of myotomy width. Although the simulation set 1 was performed with idealized conditions, i.e., perfect pan-esophageal pressurization and closed EGJ, similar conditions may be observed clinically with an incomplete myotomy or obstructive fundoplication. Simulation set 2 validates this point by showing that other contraction patterns also lead to greater deformation at myotomy site for longer myotomies than for short myotomies. In addition, by comparing different contraction patterns in *simulation set 2*, we found that peristalsis has the greatest chance of a BOM formation followed by spasm and pan-esophageal pressurization. Through group I of simulation set 3, we found that a strong EGJ tone increased the chances of BOM formation, whereas intact muscle fibers at the myotomy site reduce the likelihood formation of BOM. Although peristalsis sometimes returns postmyotomy (24), the contraction pattern postmyotomy is unpredictable. We chose peristalsis as the contraction pattern to test because it has the most adverse effect on BOM formation (as seen in simulation set 2) thereby accentuating the potential influence of EGJ tone on minimizing the chances of BOM formation. Group II of simulation set 3 showed that the chances of BOM formation are decreased in the case of POEM compared with LHM since the remnant LM fibers after POEM prevented large deformation at the myotomy site.

Implications and Future Directions

In practice, only the myotomy length is controlled while the width depends on the myotomy length. In general, a longer myotomy leads to the formation of a wider weak section. Since the effect of width on the volume accumulated inside the deformed myotomy site is negligible, our study validates the current practice of controlling only the length of myotomy to control the formation of a BOM. Identifying the LES during a myotomy procedure can be challenging. Therefore, a longer myotomy might appear to be safer choice to make sure EGJOO is no longer present. In addition, myotomies are accompanied by fundoplication, which increase the overall EGJ tone. But our simulations show that this combination of long myotomy with a strong EGJ tone possibly due to fundoplication maximizes the risk of BOM formation. Instead, effort should be made to have shorter myotomies focused at the LES and try to avoid fundoplication to minimize the chances of BOM formation. This is consistent with the initial description of BOM (6) that showed that BOM was not found in patients undergoing pneumatic dilation (essentially a short myotomy despite not being complete) but occurred frequently in patients treated with LHM and Dor fundoplasty.

Our simulations show that even with fundoplication that raises EGJ tone, shorter myotomies lead to proper bolus outflow and decrease the chances of BOM formation. This is because smaller myotomy affected regions have a higher overall esophageal wall stiffness compared with larger myotomy affected zone. Stiffer walls lead to increased intrabolus pressure, which opens the EGJ, whereas weaker walls deform easily without raising the bolus pressure, and thus, the EGJ does not open, and the bolus gets retained at the myotomy site. For the same reason, as shown by simulation set 3, if the myotomy was not transmural or continued to have some muscle fibers at the myotomy site, then the chances of BOM formation are reduced. Thus, myotomy procedures such as POEM have an advantage over LHM as they may target only the CM and leave the LM relatively intact as described by group II of simulation set 3. POEMs are especially useful for patients with type III achalasia and patients with distal esophageal spasm, where the myotomy length needs to be sufficient to include the spastic region. Hence, POEMs can go upwards of 10 cm but still be successful in retaining the myotomy wall strength sufficient to resist large deformation and aid in bolus emptying. In addition, a realtime tailored myotomy as possible with intraoperative FLIP to obtain targeted values of distensibility at the myotomy affected zone as well as at the EGJ might help in performing myotomies with lower chances of forming BOM.

Different contraction patterns as observed in different achalasia types have different effects on the deformation at the myotomy site. In addition, it has been observed that some patients with achalasia have evidence of partial peristalsis after myotomy likely due to it becoming more evident in the less dilated esophagus posttreatment (24). Because of the absence of contraction in achalasia I, the chances of BOM formation are minimal, irrespective of the myotomy length and EGJ tone after fundoplication. But, based on our simulations, patients with EGJOO with normal peristalsis and patients suffering from achalasia III have a higher risk of forming BOM with longer myotomy length and strong EGJ tone. Therefore, it might be beneficial to aim for shorter myotomy without fundoplication for such patients. Longer myotomies performed on patients with achalasia III can sometimes weaken the spastic contractions at the distal segment of the esophagus. This would reduce the chances of forming a BOM. But, on the other hand, if the myotomy is partially through the spastic segment with remnant spasm forcing bolus into the distal esophagus, it might aid in the formation of a BOM. Thus, the myotomy length should be determined in a patient-specific manner with the help of diagnostic devices such as HRM and physics-based simulations (25) that work with HRM data.

Limitations

BOM was qualitatively defined in Triggs et al. (6), but there is a lack of quantitative definition of BOM in the literature. BOMs form due to tissue remodeling over a long timeline compared with the single swallows used in our modeling. Our simulations do not account for tissue remodeling. Thus, the deformation at the myotomy site seen in our simulations is not a BOM, but rather the repetitive strain that would be exerted on the myotomy. This is a limitation of the vEsophagus model. With our simulations, we can only hypothesize that factors leading to maximum deformation at the myotomy site will also impact in the formation of a BOM over a longer period. The material properties used in the vEsophagus were motivated from experimental observations of porcine esophagus due to the lack of experimental data on the human esophagus. In addition, because of the presence of the surrounding organs, the effective distensibility of the esophagus varies along its length. These complexities were not considered in our model. In addition, the vEsophagus focuses just on the esophagus without considering the stomach. Adding a stomach to the model would increase the stiffness at the distal end of the esophagus, and the intragastric pressure will require higher intrabolus pressure to empty out the bolus. Considering these factors would increase the computation time significantly without any significant additions to our current observations. Another significant limitation of this study is that we have investigated only a few types of contraction patterns as typically might be observed. In reality, the nature of contraction varies significantly from swallow to swallow, particularly for achalasia II and III. In addition, the fully closed EGJ in simulation sets 1 and 2 are idealized scenarios. Simulating the actual physiological conditions of the wide variety of contraction patterns and EGJ tone is too computationally complex and costly to be practical. The observations from our simulations are still applicable to a wide variety of contraction patterns, but it might be worthwhile to investigate the impact of contractions on BOM formation, which are significantly different from what we discussed in this study. Finally, we did not consider gravity in our simulations although it is a factor in generating intrabolus pressure. Unfortunately, introducing gravity significantly increases the complexity of the simulations putting it beyond the scope of this work and making it a limitation of this work.

Conclusions

In conclusion, we performed in silico simulations to investigate the impact of different biomechanical factors that lead to the formation of a BOM such as dimensions of the myotomy, esophageal contraction pattern, EGJ tone, and residual state of muscle fibers at myotomy location. We found that long myotomies with greater EGJ tone and preserved peristalsis maximize the chances for BOM formation. Our simulations show that the best possible myotomy to minimize the chances of BOM formation is a short myotomy spanning only the length of the LES that is not transmural and has some structural architecture intact. This should be the approach in type II achalasia or EGJOO with propagating peristalsis that may be observed in patients with achalasia in evolution. Type I achalasia will likely not develop a BOM. Type III achalasia will most likely develop a BOM if the myotomy is partially through the spastic segment with remnant spasm forcing bolus into the distal esophagus. Although the final decision on the dimensions and modality of the myotomy will depend on multiple factors such as the type and severity of achalasia and fundoplication, our simulations using vEsophagus should be helpful in guiding the surgical plan.

APPENDIX

Mathematical Modeling of the vEsophagus

The vEsophagus was modeled as a fluid-structure interaction system using Immersed boundary (IB) method. In this method, the structure (esophagus) is represented using Lagrangian coordinates, and the fluid is represented using Eulerian coordinates. The governing equations are as follows:

$$\rho \left(\frac{\partial \boldsymbol{u}}{\partial t} + \boldsymbol{u} \cdot \nabla \boldsymbol{u} \right) = -\nabla p + \mu \nabla^2 \boldsymbol{u} + \boldsymbol{f}, \tag{1}$$

$$\nabla \cdot \mathbf{u} = 0, \tag{2}$$

$$f(\mathbf{x},t) = \int_{\Gamma} \mathbf{F}(\mathbf{s},t)\delta[\mathbf{x} - \mathbf{X}(\mathbf{s},t)]d\mathbf{s},$$
 (3)

$$\int_{\Gamma} \mathbf{F}(\mathbf{s},t) \cdot \mathbf{V}(\mathbf{s}) d\mathbf{s} = -\int_{\Gamma} \mathbf{P} : \nabla_{\mathbf{s}} \mathbf{V}(\mathbf{s}) d\mathbf{s}, \quad \forall \mathbf{V}(\mathbf{s}), \tag{4}$$

$$U(s,t) = \int_{\Omega} u(x,t)\delta[x - X(s,t)]dx,$$
 (5)

$$\int_{\Gamma} \frac{\partial \mathbf{X}}{\partial t}(\mathbf{s}, t) \cdot \mathbf{V}(\mathbf{s}) d\mathbf{s} = -\int_{\Gamma} \mathbf{U}(\mathbf{s}, t) \cdot \mathbf{V}(\mathbf{s}) d\mathbf{s}, \quad \forall \mathbf{V}(\mathbf{s}), \tag{6}$$

$$\mathbf{P} = \wp[\mathbf{X}(\cdot, t)],\tag{7}$$

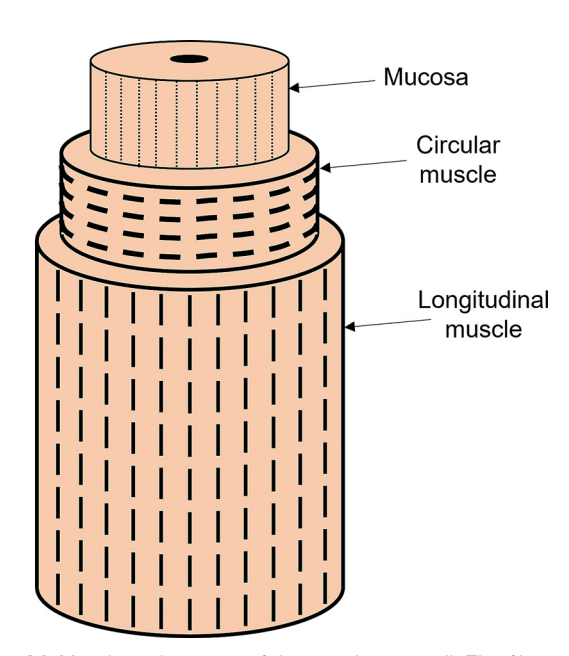


Figure A1. Muscle architecture of the esophagus wall. The fiber orientations are shown by the dashed lines. The outer longitudinal muscle fibers are oriented along the length of the esophagus, the middle circular muscle fibers are oriented in the tangential direction, and the inner mucosal layer has its fibers in the axial direction.

where Eqs. 1 and 2 are the momentum and mass conservation equations for an incompressible fluid-structure system in Eulerian description. **u** and p are the Eulerian velocity and pressure, respectively. ρ and μ are the density and viscosity of the entire system. In this case, fluid was assumed to be Newtonian and had a density and viscosity of 1,000 kg/ m³ and 10 cP, respectively. The esophageal wall was assumed to have the same density and viscosity as the fluid to avoid buoyancy effect in the IB method. Equations 3-6 are the IB fluid-structure equations, where f and F are the Eulerian and Lagrangian elastic force density, respectively. *U,X*, and **P** are the structure velocity, position, and first Piola-Kirchhoff stress, respectively. *Equation 7* is a generic form representing the relation between **P** and the hyperelastic strain energy function that define the elastic behavior of the structure.

In IB method, the whole vEsophagus model is immersed in a fluid box that include the fluid bolus inside the esophagus. The proximal end of the vEsophagus is fixed with zero outflow to account for the closed UES once the bolus is inside the esophagus. For *simulation set 1* and 2, the lower

Table A1. Specific physiological scenarios corresponding to each of the simulation cases

Case Number	Myotomy Dimensions	Physiological Scenario
1	Simulation set 1: Pan-esophageal contraction, fully occluded EGJ Length: 60 mm, width: 7 mm	Type II achalasia with incomplete myotomy or tight fundoplication
<i>2</i> 3	Length: 90 mm, width: 7 mm Length: 30 mm, width: 7 mm	
4	Length: 60 mm, width: 4 mm	
5	Length: 60 mm, width: 10 mm	
Case Number	Details Simulation set 2	Physiological Scenario
1	Peristalsis (normal), standard myotomy	EGJOO
2 3	Very weak contraction (achalasia I), standard myotomy Pan-esophageal contraction (achalasia II), standard myotomy	Type I achalasia Type II achalasia
4	Proximal peristalsis transitions with distal spasm (achalasia III), standard myotomy	Type III achalasia
5	Peristalsis (normal), short myotomy	EGJOO
6	Very weak contraction (achalasia I), short myotomy	Type I achalasia
7	Pan-esophageal contraction (achalasia II), short myotomy	Type II achalasia
8	Proximal peristalsis transitions with distal spasm (achalasia III), short myotomy	Type III achalasia
Case Number	Details Simulation set 3: group I	Physiological Scenario
1	Standard myotomy length (6 cm); no EGJ tone; myotomy affected zone walled by mucosa only; contraction type: normal peristalsis	Long LHM with no fundoplication in patient with EGJOO
2	Standard myotomy length (6 cm); with an EGJ tone; myotomy affected zone walled by mucosa only; contraction type: normal peristalsis	Long LHM with tight fundoplica- tion in patient with EGJOO
3	Standard myotomy length (6 cm); with an EGJ tone; myotomy affected zone walled by mucosa and weakened muscle layers (the strength of the muscle fibers were reduced by 99% but the matrix of the muscle layers were intact at the myotomy site); contraction type: normal peristalsis	Partially healed esophagus after long LHM with tight fundoplica- tion in patient with EGJOO
4	Short myotomy length (3 cm); no EGJ tone; myotomy affected zone walled by mucosa only; contraction type: normal peristalsis	Short LHM with no fundoplication in patient with EGJOO
5	Short myotomy length (3 cm); with an EGJ tone; myotomy affected zone walled by mucosa only; contraction type: normal peristalsis	Short LHM with tight fundoplica- tion in patient with EGJOO
6	Short myotomy length (3 cm); with an EGJ tone; myotomy affected zone walled by mucosa and weakened muscle layers (the strength of the muscle fibers were reduced by 99% but the matrix of the muscle layers were intact at the myotomy site); contraction type: normal peristalsis	Partially healed esophagus after short LHM with tight fundoplica- tion in patient with EGJOO
Details	Physiological Scenario	
Simulation set 3: grou		
POEM length: 12 cm; LM intact at the myotomy site while CM	Esophagus after POEM	
fibers were broken, and CM		
matrix strength reduced 100-		
fold; with an EGJ tone; contrac-		
tion type: normal peristalsis		

CM, circular muscle; EGJ, esophagogastric junction; EGJOO, esophagogastric junction outflow obstruction; LHM, laparoscopic Heller myotomy; LM, longitudinal muscle; POEM, Peroral endoscopic myotomy.

end of the esophagus is also fixed to model the extreme scenario of fully occluded EGJ. For simulation set 3, the lower end of the esophagus is free to move. In all these simulations, the sides of the esophagus do not have any constraint and are free to move. We have imposed zero velocity boundary condition at the upper surface of the fluid domain. The same boundary condition was also imposed at the lower surface for simulation sets 1 and 2. For simulation set 3, the lower fluid surface has free outflow boundary condition. The other four outer surfaces of the fluid domain for all these simulations have free outflow boundary condition enforced.

vEsophagus Wall Properties

The wall of the vEsophagus was modeled as a composite of hyperelastic materials with each layer composed of fibers embedded in a matrix as shown in Fig. A1. The elastic behavior of each layer is due to the combined influence of the fibers and matrix. The material model used for the mucosal layer is as follows:

$$\psi^{\text{mucosa}} = \psi^{\text{mucosa}}_{\text{matrix}} + \psi^{\text{mucosa}}_{\text{fiber}},$$
(8)

$$\psi_{\text{matrix}}^{\text{mucosa}} = \frac{C_o}{2} (I_1 - 1), \tag{9}$$

$$\psi_{\text{fiber}}^{\text{mucosa}} = \frac{C_1}{2} \left(\sqrt{I_4^{\text{mucosa}}} - 1 \right)^2, \tag{10}$$

where I_1 = tr(\mathbb{C}), $I_{\Delta}^{\text{mucosa}} = \mathbb{C} : (a^{\text{mucosa}} \otimes a^{\text{mucosa}})$, and a^{mucosa} is the unit vector along the axial direction ψ^{mucosa} , ψ^{mucosa}_{matrix} , and $\psi_{\text{fiber}}^{\text{mucosa}}$ are the total, matrix, and fiber strain energy function of the mucosa, respectively. The matrix is modeled as a Neo-Hookean material, and the fibers are modeled as a bilinear model. C is the right Cauchy–Green tensor. In this model, C_0 = 0.004 kPa and C_1 = 0.04 kPa.

The material model used for the muscle layers are as follows:

$$\psi^{\text{muscle}} = \psi^{\text{muscle}}_{\text{matrix}} + \psi^{\text{muscle}}_{\text{fiber}}, \tag{11}$$

$$\psi_{\text{matrix}}^{\text{muscle}} = \frac{C_2}{2}(I_1 - 1), \tag{12}$$

$$\psi_{\text{fiber}}^{\text{muscle}} = \frac{C_3}{2} \left(\frac{\sqrt{I_4^{\text{muscle}}}}{\lambda} - 1 \right)^2, \tag{13}$$

where $I_4^{
m muscle}=\mathbb{C}:(\pmb{a}^{
m muscle}\otimes \pmb{a}^{
m muscle})$, and $\pmb{a}^{
m muscle}$ is the unit vector along the circumferential and axial direction for circular muscles (CMs) and longitudinal muscles (LMs), respectively. ψ^{muscle} , ψ^{muscle}_{matrix} , and ψ^{muscle}_{fiber} are the total, matrix, and fiber strain energy function of the muscle layers, respectively. The parameter λ induces a contraction in the muscle fibers when $\lambda < 1$. λ lies between 0 and 1, with a smaller value indicating a tighter contraction. The CM and LM are significantly stiffer than the mucosal layer. In this model, $C_2 = 0.4$ kPa and C_3 = 40 kPa. Although we used the same strength for the longitudinal and circular muscles fibers (C_3) , the net strength of each muscle layer depends on both the strength of the fibers and their orientation (as specified by a^{muscle}).

Contraction Patterns

Based on the contractile behavior of the esophagus, it is possible to distinguish different esophageal motility disorders. A

normal subject exhibits normal peristalsis. Patients with achalasia type I do not show any prominent contractile behavior. Patients with achalasia type II experience pan-esophageal pressurization. Patients with achalasia type III have a huge variability in the contraction pattern, but typically they exhibit a combination of peristalsis in the proximal esophagus and spasm in the distal esophagus. In order simulations, the contraction is implemented by specifying λ . The mathematical details of the different contraction patterns discussed in the three simulation sets are described below.

Peristaltic contraction.

 $\lambda_{peristalsis} =$

$$\begin{cases} 1 & \text{if } t \leq \frac{L-z}{c}, \\ 1 - \lambda_0 e^{-0.5(z-ct)^2/w^2} & \text{if } \frac{L-z}{c} < t < \frac{L-z}{c} + \frac{\Delta L}{c}, \\ 1 & \text{if } t \geq \frac{L-z}{c} + \frac{\Delta L}{c}, \end{cases}$$

$$(14)$$

where z = 0 at the distal end of the esophagus and z = L at the proximal end, L is the length of the esophagus, c is the speed of the peristaltic contraction, ΔL is the length of the contracting segment, λ_0 is the amplitude of the activation parameter, and w is a parameter that specifies the width of the Gaussian function that controls the nature of the contraction. In our simulations, we used $\lambda_0 = 0.4$, c = 200 mm/s, $\Delta L = 60$ mm, and w = 15 mm.

Pan-esophageal pressurization.

 $\lambda_{panesophageal} =$

$$\begin{cases} 1 & \text{if } Z < 0, \\ 1 - \gamma(t)\lambda_o \left[1 - \cos\left(\frac{2\pi Z}{l_1}\right) \right] & \text{if } 0 \le Z < \frac{l_1}{2}, \\ 1 - 2\gamma(t)\lambda_o & \text{if } \frac{l_1}{2} \le Z < \frac{l_1}{2} + l_2, \\ 1 - \gamma(t)\lambda_o \left[1 + \cos\left(\frac{2\pi \left(Z - \frac{l_1}{2} - l_2\right)}{l_2}\right) \right] & \text{if } \frac{l_1}{2} + l_2 \le Z < \frac{l_1}{2} + l_2 + \frac{l_3}{2}, \\ 1 & \text{if } \frac{l_1}{2} + l_2 + \frac{l_3}{2} \le Z, \end{cases}$$

$$(15)$$

where Z = L - z, $0 < \gamma(t) < 1$ is the parameter that determines the speed at which the pressurization occurs. l_1 and l_3 are the length segments at the proximal and distal ends of the esophagus, where the maximal amplitude of the contraction strength reduces to zero at the two ends. l_2 is the length segment at the center of the esophagus where the maximum pressurization acts. λ_o is the amplitude of the contraction, and in our simulations, we used $\lambda_0 = 0.85$.

Proximal peristalsis with distal spasm.

To implement this contraction, we enforce $\lambda_{peristal}$ to the proximal half of the esophagus with a reduction in strength at the transition between the proximal and distal portions of the esophagus. In the distal half of the esophagus, the value of λ is specified as follows:

$$\lambda_{spasm} = \alpha \lambda_{panesophageal},$$
 (16)

where $\alpha = \frac{1}{4} \left[3 + \sin \left(\frac{2n\pi z_d}{L_d} \right) \right]$, L_d is the length of the distal half of the esophagus, z_d is the coordinate along the length of the esophagus starting from the middle of the esophagus to



its distal end, and n is the number of high spastic zones. In our simulations, we have used n = 3. The maximum amplitude of spasm in the distal esophagus was $\lambda_0 = 0.75$. All the simulations described in this paper correspond to specific physiological scenarios. The details of these physiological scenarios are provided in Table A1.

GRANTS

This work was supported by National Institute of Diabetes and Digestive and Kidney Diseases (NIDDK) Grants R01-DK079902 and P01-DK117824 (to J. E. Pandolfino) and by the National Science Foundation (NSF) Grants OAC 1450374 and OAC 1931372 (to N. A. Patankar).

DISCLOSURES

Peter J. Kahrilas and John E. Pandolfino hold shared intellectual property rights and ownership surrounding FLIP panometry systems, methods, and apparatus with Medtronic Inc. Dustin A. Carlson: Medtronic (Speaking, Consulting). Wenjun Kou: Crospon, Inc. (Consulting). Peter J. Kahrilas: Ironwood (Consulting). John E. Pandolfino: Crospon, Inc (stock options), Given Imaging (Consultant, Grant, Speaking), Sandhill Scientific (Consulting, Speaking), Takeda (Speaking), Astra Zeneca (Speaking), Medtronic (Speaking, Consulting), Torax (Speaking, Consulting), Ironwood (Consulting), Impleo (Grant). No conflicts of interest, financial or otherwise, are declared by the authors.

AUTHOR CONTRIBUTIONS

S.H., S.A., W.K., P.J.K., J.E.P., and N.A.P. conceived and designed research; S.H. performed experiments; S.H., R.A.J.C., J.R.T., D.A.C., A.A.A., and E.S.H. analyzed data; S.H., R.A.J.C., D.A.C., P.J.K., J.E.P., and N.A.P. interpreted results of experiments; S.H. prepared figures; S.H. drafted manuscript; S.H., P.J.K., J.E.P., and N.A.P. edited and revised manuscript; S.H., P.J.K., J.E.P., and N.A.P. approved final version of manuscript.

REFERENCES

- Yadlapati R, Kahrilas PJ, Fox MR, Bredenoord AJ, Prakash Gyawali C, Roman S, et al. Esophageal motility disorders on high-resolution manometry: Chicago classification version Neurogastroenterol Motil 33: e14058, 2021, doi:10.1111/nmo.14113.
- Kahrilas PJ, Bredenoord AJ, Fox M, Gyawali CP, Roman S, Smout AJPM, Pandolfino JE; International High Resolution Manometry Working Group. The Chicago Classification of esophageal motility disorders, v3.0. Neurogastroenterol Motil 27: 160-174, 2015. doi:10. 1111/nmo.12477.
- Samo S, Carlson DA, Gregory DL, Gawel SH, Pandolfino JE, Kahrilas PJ. Incidence and Prevalence of Achalasia in Central Chicago, 2004-2014, since the widespread use of high-resolution manometry. Clin Gastroenterol Hepatol 15: 366-373, 2017. doi:10.1016/j.cgh.2016.08.030.
- Triadafilopoulos G, Boeckxstaens GE, Gullo R, Patti MG, Pandolfino JE, Kahrilas PJ, Duranceau A, Jamieson G, Zaninotto G. The Kagoshima consensus on esophageal achalasia. Dis Esophagus 25: 337-348, 2012. doi:10.1111/j.1442-2050.2011.01207.x.
- Campos GM, Vittinghoff E, Rabl C, Takata M, Gadenstätter M, Lin F, Ciovica R. Endoscopic and surgical treatments for achalasia: a systematic review and meta-analysis. Ann Surg 249: 45-57, 2009. doi:10.1097/SLA.0b013e31818e43ab.
- Triggs JR. Krause AJ. Carlson DA. Donnan EN. Campagna RAJ. Jain AS, Kahrilas PJ, Hungness ES, Pandolfino JE. Blown-out myotomy: an adverse event of laparoscopic Heller myotomy and peroral endoscopic myotomy for achalasia. Gastrointest Endosc 93: 861-868.e1, 2021. doi:10.1016/j.gie.2020.07.041.

- Jain AS, Carlson DA, Triggs J, Tye M, Kou W, Campagna R, Hungness E, Kim D, Kahrilas PJ, Pandolfino JE. Esophagogastric junction distensibility on functional lumen imaging probe topography predicts treatment response in achalasia—anatomy matters!. Am J Gastroenterol 114: 1455-1463, 2019. doi:10.14309/ajg.000000000000137.
- Kou W, Pandolfino JE, Kahrilas PJ, Patankar NA. Studies of abnormalities of the lower esophageal sphincter during esophageal emptying based on a fully coupled bolus-esophageal-gastric model. Biomech Model Mechanobiol 17: 1069-1082, 2018. doi:10.1007/ s10237-018-1014-v.
- Kou W, Griffith BE, Pandolfino JE, Kahrilas PJ, Patankar NA. A continuum mechanics-based musculo-mechanical model for esophageal transport. J Comput Phys 348: 433-459, 2017. doi:10.1016/j. icp.2017.07.025.
- Yang W, Fung TC, Chian KS, Chong CK. Viscoelasticity of esophageal tissue and application of a QLV model. J Biomech Eng 128: 909-916, 2006. doi:10.1115/1.2372473.
- Yang W, Fung TC, Chian KS, Chong CK. Investigations of the viscoelasticity of esophageal tissue using incremental stress-relaxation test and cyclic extension test. J Mech Med Biol 06: 261-272, 2006. doi:10.1142/S0219519406001984.
- Puckett JL, Bhalla V, Liu J, Kassab G, Mittal RK. Oesophageal wall stress and muscle hypertrophy in high amplitude oesophageal contractions. Neurogastroenterol Motil 17: 791-799, 2005. doi:10.1111/ j.1365-2982.2005.00693.x.
- Jacob P, Kahrilas PJ, Logemann JA, Shah V, Ha T. Upper esophageal sphincter opening and modulation during swallowing. Gastroenterology 97: 1469-1478, 1989. doi:10.1016/0016-5085(89)90391-0.
- Lang IM, Shaker R. Anatomy and physiology of the upper esophageal sphincter. Am J Med 103: 50S-55S, 1997. doi:10.1016/s0002-9343(97)00323-9.
- Natali AN, Carniel EL, Gregersen H. Biomechanical behaviour of oesophageal tissues: material and structural configuration, experimental data and constitutive analysis. Med Eng Phys 31: 1056-1062, 2009. doi:10.1016/j.medengphy.2009.07.003.
- Yang W, Fung TC, Chian KS, Chong CK. Directional, regional, and layer variations of mechanical properties of esophageal tissue and its interpretation using a structure-based constitutive model. J Biomech Eng 128: 409-418, 2006. doi:10.1115/1.2187033.
- Kou W, Pandolfino JE, Kahrilas PJ, Patankar NA. Could the peristaltic transition zone be caused by non-uniform esophageal muscle fiber architecture? A simulation study. Neurogastroenterol Motil 29: e13022, 2017. doi:10.1111/nmo.13022.
- Kou W, Pandolfino JE, Kahrilas PJ, Patankar NA. Simulation studies of the role of esophageal mucosa in bolus transport. Biomech Model Mechanobiol 16: 1001-1009, 2017. doi:10.1007/s10237-016-0867-1.
- Yang W, Fung TC, Chian KS, Chong CK. 3D mechanical properties of the layered esophagus: experiment and constitutive model. JBiomech Eng 128: 899-908, 2006. doi:10.1115/1.2354206.
- Pouderoux P, Lin S, Kahrilas PJ. Timing, propagation, coordination, and effect of esophageal shortening during peristalsis. Gastroenterology 112: 1147-1154, 1997. doi:10.1016/s0016-5085(97)70125-2.
- Mittal RK, Padda B, Bhalla V, Bhargava V, Liu J. Synchrony between circular and longitudinal muscle contractions during peristalsis in normal subjects. Am J Physiol Gastrointest Liver Physiol 290: G431-G438, 2006. doi:10.1152/ajpgi.00237.2005.
- Griffith BE, Hornung RD, McQueen DM, Peskin CS. An adaptive, formally second order accurate version of the immersed boundary method. J Comput Phys 223: 10-49, 2007. doi:10.1016/j.jcp.2006.08.019.
- Childs H, Brugger E, Whitlock B, Meredith J, Ahern S, Pugmire D, Biagas K, Miller M, Harrison C, Weber GH, Krishnan H, Fogal T, Sanderson A, Garth C, Bethel EW, Camp D, Rubel O, Durant M, Favre JM, Navratil P. Vislt: an end-user tool for visualizing and analyzing very large data. In: High Performance Visualization-Enabling Extreme-Scale Scientific Insight, edited by Bethel EW, Childs H, Hansen C. Boca Raton, FL: CRC Press, 2012 p. 357-372
- Roman S, Kahrilas PJ, Mion F, Nealis TB, Soper NJ, Poncet G, Nicodème F, Hungness E, Pandolfino JE. Partial recovery of peristalsis after myotomy for achalasia: more the rule than the exception. JAMA Surg 148: 157-164, 2013. doi:10.1001/2013.jamasurg.38.
- Halder S, Acharya S, Kou W, Kahrilas PJ, Pandolfino JE, Patankar NA. Mechanics informed fluoroscopy of esophageal transport. Biomech Model Mechanobiol 20: 925-940, 2021. doi:10.1007/ s10237-021-01420-0.